Scatter Estimation for PET Reconstruction

M. Magdics, L. Szirmay-Kalos, B. Tóth, Á. Csendesi[1], A. Penzov[2]

[1] Budapest University of Technology and Economics, Hungary
[2] Institute of Information and Communication Technologies, BAS, Bulgaria

Abstract. This paper presents a Monte Carlo scatter estimation algorithm for Positron Emission Tomography (PET) where positron-electron annihilations induce photon pairs that fly independently in the medium and eventually get absorbed in the detector grid. The path of the photon pair will be a *polyline* defined by the detector hits and scattering points where one of the photons changed its direction. The values measured by detector pairs will then be the total contribution, i.e. the integral of such polyline paths of arbitrary length. This integral is evaluated with Monte Carlo quadrature, using a sampling strategy that is appropriate for the graphics processing unit (GPU) that executes the process. We consider the contribution of photon paths to each pair of detectors as an integral over the Cartesian product set of the volume. This integration domain is sampled globally, i.e. a single polyline will represent all annihilation events occurred in any of its points. Furthermore, line segments containing scattering points will be reused for all detector pairs, which allows us to significantly reduce the number of samples. The scatter estimation is incorporated into a PET reconstruction algorithm where the scattered term is subtracted from the measurements.

1 Introduction

In positron emission tomography (PET) we need to find the spatial intensity distribution of positron–electron annihilations. During an annihilation event, two oppositely directed 511 keV photons are produced [Gea07]. We collect the number of simultaneous photon hits in detector pairs, also called *Lines Of Responses* or *LORs*: $(y_1, y_2, \ldots, y_{N_{LOR}})$. The required output of the reconstruction method is the *emission density* function $x(\boldsymbol{v})$ that describes the number of photon pairs (i.e. the annihilation events) born in a unit volume around point $\boldsymbol{v}$. Tomography reconstruction algorithms are usually iterative. They start with an initial emission density, compute the detector response by simulating the photon transport and update the emission density taking into account the actual simulated and the measured detector responses [SV82]. Before being detected in the detectors, photons might interact with the matter in many ways, but in our energy range and for living organs only Compton scattering and the photoelectric absorption are relevant. The probability of scattering in unit distance is the *scattering cross section* σ_s. When scattering happens, there is a unique correspondence between the relative scattered energy and the cosine of the scattering angle θ, as defined

by the *Compton formula*:

$$\epsilon = \frac{1}{1 + \epsilon_0(1 - \cos\theta)},$$

where $\epsilon = E_1/E_0$ expresses the ratio of the scattered energy E_1 and the incident energy E_0, and $\epsilon_0 = E_0/(m_e c^2)$ is the incident photon energy relative to the energy of the electron. The differential of the *scattering cross section*, i.e. the probability density that the photon is scattered from direction $\boldsymbol{\omega}'$ into differential solid angle $\mathrm{d}\omega$ in direction $\boldsymbol{\omega}$, is given by the *Klein-Nishina formula* [Yan08]:

$$\frac{\mathrm{d}\sigma_s(\boldsymbol{v}, \cos\theta, \epsilon_0)}{\mathrm{d}\omega} = \frac{r_e^2 C(\boldsymbol{v})}{2}(\epsilon + \epsilon^3 - \epsilon^2 \sin^2\theta),$$

where $\cos\theta = \boldsymbol{\omega} \cdot \boldsymbol{\omega}'$, $C(\boldsymbol{v})$ is the electron density, and $r_e = 2.82 \cdot 10^{-15}$ [m] is the classical electron radius. The Klein-Nishina formula defines the product of the scattering cross section $\sigma_s(\boldsymbol{v}, \epsilon_0)$ and the conditional probability density of the scattering direction. The scattering cross section can be obtained as the directional integral of the Klein-Nishina formula over the whole directional sphere:

$$\sigma_s(\boldsymbol{v}, \epsilon_0) = \int_{\Omega} \frac{\mathrm{d}\sigma_s(\boldsymbol{v}, \cos\theta, \epsilon_0)}{\mathrm{d}\omega} \mathrm{d}\omega = \frac{r_e^2 C(\boldsymbol{v})}{2} \sigma_s^0(\epsilon_0) \tag{1}$$

where Ω is the directional sphere and σ_s^0 is the *normalized scattering cross section*:

$$\sigma_s^0(\epsilon_0) = \int_{\Omega} \epsilon + \epsilon^3 - \epsilon^2 \sin^2\theta \mathrm{d}\omega = -2\pi \int_{-1}^{1} \epsilon + \epsilon^3 - \epsilon^2 \sin^2\theta \mathrm{d}\cos\theta.$$

The ratio of the Klein-Nishina formula and the scattering cross section is the *phase function*, which defines the probability density of the reflection direction, provided that reflection happens:

$$P_{KN}(\cos\theta, \epsilon_0) = \frac{\mathrm{d}\sigma_s}{\mathrm{d}\omega}/\sigma_s = \frac{\epsilon + \epsilon^3 - \epsilon^2 \sin^2\theta}{\sigma_s^0(\epsilon_0)}.$$

The absorption cross section $\sigma_a(\epsilon_0)$ due to the photoelectric effect is approximately inversely proportional to the cube of the photon energy, thus

$$\sigma_a(\boldsymbol{v}, \epsilon_0) \approx \frac{\mathrm{const}}{E^3} = \frac{\sigma_a(\boldsymbol{v}, 1)}{\epsilon_0^3}. \tag{2}$$

The proportionality ratio $\sigma_a(\boldsymbol{v}, 1)$ depends on the material compounds and grows rapidly (with a power between 4 and 5) with the atomic number of the elements.

2 Previous work

A physically plausible scatter correction needs photon transport simulation and the evaluation of high-dimensional integrals in photon path space. As classical quadrature rules fail in higher dimensions due to the *curse of dimensionality*, these high-dimensional integrals are estimated by Monte Carlo or quasi-Monte Carlo methods [SK08]. Unfortunately, available Monte Carlo tools, like Geant4/GATE [Gea07,ABB+04], MCNP[3], SimSet[4], PeneloPET [EHV+06], are too general, and therefore not optimized for the particular task and not suitable for GPU execution. Thus, they are too slow to be incorporated into an on-line iterative reconstruction.

For effective simulation, we run our algorithm on the graphics processing unit (GPU), which is a massively parallel supercomputer. It can reach teraflops performance if its quasi-SIMD architecture is respected, i.e. if threads execute the same instruction sequence with no communication. The direct simulation of the photon transport would not meet this requirement since different photons may end up in the same detector which needs synchronized writes. Thus, we consider the adjoint problem and take a detector oriented viewpoint. For efficient evaluation, we transform the integral over the path space to a volumetric integral.

3 Scatter estimation

If we consider photon scattering, the path of the photon pair will be a *polyline* containing the emission point somewhere inside one of its line segments (Fig. 1). This polyline includes scattering points $\boldsymbol{s}_1, \ldots, \boldsymbol{s}_S$ where one of the photons changed its direction in addition to detector hit points $\boldsymbol{z}_1 = \boldsymbol{s}_0$ and $\boldsymbol{z}_2 = \boldsymbol{s}_{S+1}$. The values measured by detector pairs will then be the total contribution, i.e. the integral of such polyline paths of arbitrary length.

We consider the contribution of photon paths as an integral over the Cartesian product set of the volume. This integration domain is sampled globally, i.e. a single sample is used for the computation of all detector pairs. Sampling parts of photon paths globally and *reusing* a partial path for all detector pairs allow us to significantly reduce the number of samples.

To express the contribution of a polyline path, we take its line segments one-by-one and consider a line segment as a *virtual LOR* with two virtual detectors of locations, $\boldsymbol{s}_{i-1}$ and $\boldsymbol{s}_i$, and of differential areas projected perpendicularly to the line segment, $\mathrm{d}A^{\perp}_{i-1}$ and $\mathrm{d}A^{\perp}_{i}$ (Fig. 1). The contribution of a virtual LOR at its endpoints, i.e. the expected number of photon pairs going through $\mathrm{d}A^{\perp}_{i-1}$ and $\mathrm{d}A^{\perp}_{i}$ is $C(\boldsymbol{s}_{i-1}, \boldsymbol{s}_i)\mathrm{d}A^{\perp}_{i-1}\mathrm{d}A^{\perp}_{i}$, where contribution C is the product of several factors:

$$C(\boldsymbol{s}_{i-1}, \boldsymbol{s}_i) = G(\boldsymbol{s}_{i-1}, \boldsymbol{s}_i)X(\boldsymbol{s}_{i-1}, \boldsymbol{s}_i)T_1(\boldsymbol{s}_{i-1}, \boldsymbol{s}_i)B_1(\boldsymbol{s}_{i-1}, \boldsymbol{s}_i),$$

[3] http://mcnp-green.lanl.gov/

[4] http://depts.washington.edu/simset/html/simset_main.html

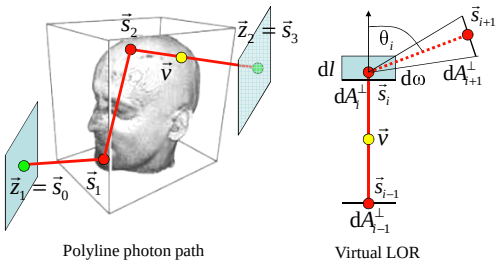

Fig. 1. The scattered photon path is a polyline (left) made of virtual LORs (right). The left figure depicts the case of $S = 2$.

where $G(\boldsymbol{s}_{i-1}, \boldsymbol{s}_i)$ is the *geometry factor*, $X(\boldsymbol{s}_{i-1}, \boldsymbol{s}_i)$ is the *total emission* along the line segment, $T_{\epsilon_0}(\boldsymbol{s}_{i-1}, \boldsymbol{s}_i)$ is the *total attenuation due to out-scattering*, and $B_{\epsilon_0}(\boldsymbol{s}_{i-1}, \boldsymbol{s}_i)$ is the *total attenuation due to photoelectric absorption*, assuming photon energy ϵ_0:

$$G(\boldsymbol{s}_{i-1}, \boldsymbol{s}_i) = \frac{1}{|\boldsymbol{s}_{i-1} - \boldsymbol{s}_i|^2}, \qquad X(\boldsymbol{s}_{i-1}, \boldsymbol{s}_i) = \frac{1}{2\pi} \int_{\boldsymbol{s}_{i-1}}^{\boldsymbol{s}_i} x(\boldsymbol{l}) \mathrm{d}l,$$

$$T_{\epsilon_0}(\boldsymbol{s}_{i-1}, \boldsymbol{s}_i) = e^{-\int_{\boldsymbol{s}_{i-1}}^{\boldsymbol{s}_i} \sigma_s(\boldsymbol{l}, \epsilon_0) \mathrm{d}l}, \qquad B_{\epsilon_0}(\boldsymbol{s}_{i-1}, \boldsymbol{s}_i) = e^{-\int_{\boldsymbol{s}_{i-1}}^{\boldsymbol{s}_i} \sigma_a(\boldsymbol{l}, \epsilon_0) \mathrm{d}l}$$

In the line segment of the emission, the original photon energy has not changed yet, thus $\epsilon_0 = 1$.

Suppose that scattering happens around end point $\boldsymbol{s}_i$ of the virtual LOR in differential volume $\mathrm{d}s_i = \mathrm{d}A^{\perp}_i \mathrm{d}l$, i.e. at run length $\mathrm{d}l$ (right of Fig. 1). Let us extend this virtual LOR by a single scattering step to form polyline $\boldsymbol{s}_{i-1}, \boldsymbol{s}_i, \boldsymbol{s}_{i+1}$. The probability that the photon scatters along distance $\mathrm{d}l$ and its new direction is in solid angle $\mathrm{d}\omega$ is differential cross section $\mathrm{d}\sigma_s(\boldsymbol{s}_i, \cos\theta_i, \epsilon_0^{(i)})/\mathrm{d}\omega \cdot \mathrm{d}l$ where θ_i is the scattering angle. The scattered photon will go along virtual LOR $(\boldsymbol{s}_i, \boldsymbol{s}_{i+1})$ with differential area $\mathrm{d}A^{\perp}_{i+1}$ at its end if area $\mathrm{d}A^{\perp}_{i+1}$ subtends solid angle $\mathrm{d}\omega$, that is:

$$\mathrm{d}\omega = \frac{\mathrm{d}A^{\perp}_{i+1}}{|\boldsymbol{s}_i - \boldsymbol{s}_{i+1}|^2}.$$

Upon scattering the photon changes its energy to

$$\epsilon_0^{(i+1)} = \frac{\epsilon_0^{(i)}}{1 + \epsilon_0^{(i)}(1 - \cos\theta)}.$$

This photon arrives at the other end of this virtual LOR if there is no further collision, which happens with probability $T_{\epsilon_0^{(i+1)}}(\boldsymbol{s}_i, \boldsymbol{s}_{i+1}) B_{\epsilon_0^{(i+1)}}(\boldsymbol{s}_i, \boldsymbol{s}_{i+1})$.

Summarizing, the expected number of photon pairs born between $\boldsymbol{s}_{i-1}$ and $\boldsymbol{s}_i$ and reaching differential areas $\mathrm{d}A^{\perp}_{i-1}$ and $\mathrm{d}A^{\perp}_{i+1}$ via scattering at differential

volume $\mathrm{d}s_i = \mathrm{d}l \cdot \mathrm{d}A_i^{\perp}$ is:

$$C(\boldsymbol{s}_{i-1}, \boldsymbol{s}_i) \frac{\mathrm{d}\sigma_s(\boldsymbol{s}_i, \cos\theta_i, \epsilon_0^{(i)})}{\mathrm{d}\omega} T_{\epsilon_0^{(i+1)}}(\boldsymbol{s}_i, \boldsymbol{s}_{i+1}) B_{\epsilon_0^{(i+1)}}(\boldsymbol{s}_i, \boldsymbol{s}_{i+1}) \mathrm{d}A_{i-1}^{\perp} \mathrm{d}s_i \mathrm{d}A_{i+1}^{\perp}.$$

The integral of the contributions of paths of S scattering points is the product of these factors. For example, the integral of the contribution of paths of one scattering point is

$$\tilde{y}_L^{(1)} = \int_{D_1} \int_{D_2} \int_{\mathcal{V}} \cos\theta^{(0)} \cos\theta^{(2)} \frac{\mathrm{d}\sigma_s(\boldsymbol{s}, \cos\theta, 1)}{\mathrm{d}\omega} \mathcal{P}(\boldsymbol{z}_1, \boldsymbol{s}, \boldsymbol{z}_2) \mathrm{d}s \mathrm{d}z_2 \mathrm{d}z_1$$

where $\theta^{(0)}$ is the angle between the first detector's normal and the direction of $\boldsymbol{z}_1$ to $\boldsymbol{s}$, $\theta^{(2)}$ is the angle between the second detector's normal and the direction of $\boldsymbol{z}_2$ to $\boldsymbol{s}$, and $\mathcal{P}(\boldsymbol{z}_1, \boldsymbol{s}, \boldsymbol{z}_2)$ is the contribution of this polyline:

$$\mathcal{P}(\boldsymbol{z}_1, \boldsymbol{s}, \boldsymbol{z}_2) = C(\boldsymbol{z}_1, \boldsymbol{s}) T_{\epsilon_0}(\boldsymbol{s}, \boldsymbol{z}_2) B_{\epsilon_0}(\boldsymbol{s}, \boldsymbol{z}_2) + T_{\epsilon_0}(\boldsymbol{z}_1, \boldsymbol{s}) B_{\epsilon_0}(\boldsymbol{z}_1, \boldsymbol{s}) C(\boldsymbol{s}, \boldsymbol{z}_2). \quad (3)$$

The photon's energy level ϵ_0 is obtained from the Compton formula for scattering angle θ formed by directions $\boldsymbol{s} - \boldsymbol{z}_1$ and $\boldsymbol{z}_2 - \boldsymbol{s}$.

When the attenuation is computed, we should take into account that the photon energy changes along the polyline and the scattering cross section also depends on this energy, thus different cross section values should be integrated when the annihilations on a different line segment are considered. As we wish to reuse the line segments and not to repeat ray-marching redundantly, each line segment is marched only once assuming photon energy $\epsilon_0 = 1$, and attenuations T_1 and B_1 for this line segment is computed. Then, when the place of annihilation is taken into account and the real value of the photon energy ϵ_0 is obtained, initial attenuations T_1 and B_1 are transformed. The transformation is based on the decomposition of equations (1) and (2):

$$\sigma_s(\boldsymbol{l}, \epsilon_0) = \sigma_s(\boldsymbol{l}, 1) \cdot \frac{\sigma_s^0(\epsilon_0)}{\sigma_s^0(1)}, \qquad \sigma_a(\boldsymbol{l}, \epsilon_0) = \frac{\sigma_a(\boldsymbol{l}, 1)}{\epsilon_0^3}.$$

Using this relation, we can write

$$T_{\epsilon_0} = e^{-\int_{\boldsymbol{s}_{i-1}}^{\boldsymbol{s}_i} \sigma_s(\boldsymbol{l}, \epsilon_0) \mathrm{d}l} = e^{-\frac{\sigma_s^0(\epsilon_0)}{\sigma_s^0(1)} \int_{\boldsymbol{s}_{i-1}}^{\boldsymbol{s}_i} \sigma_s(\boldsymbol{l}, 1) \mathrm{d}l} = T_1^{\frac{\sigma_s^0(\epsilon_0)}{\sigma_s^0(1)}}.$$

$$B_{\epsilon_0} = e^{-\int_{\boldsymbol{s}_{i-1}}^{\boldsymbol{s}_i} \sigma_a(\boldsymbol{l}, \epsilon_0) \mathrm{d}l} = e^{-\frac{1}{\epsilon_0^3} \int_{\boldsymbol{s}_{i-1}}^{\boldsymbol{s}_i} \sigma_a(\boldsymbol{l}, 1) \mathrm{d}l} = B_1^{\frac{1}{\epsilon_0^3}}.$$

The energy dependence of the cross section $\sigma^0(\epsilon_0)$ is a scalar function, which can be pre-computed and stored in a table.

4 High-dimensional quadrature computation

In the previous section we concluded that the scattered contribution is a sequence of increasing dimensional integrals. Numerical quadratures generate M discrete samples $\boldsymbol{u}_1, \boldsymbol{u}_2, \ldots, \boldsymbol{u}_M$ in the domain of the integration and approximate the integral as:

$$\int f(\boldsymbol{u}) \mathrm{d}\boldsymbol{u} \approx \frac{1}{M} \sum_{j=1}^{M} \frac{f(\boldsymbol{u}_j)}{p(\boldsymbol{u}_j)} \tag{4}$$

where $p(\boldsymbol{u}_j)$ is a density of samples. In the integral of the contribution, a sample $\boldsymbol{u}_j$ is a photon path connecting two detectors via S scattering points and containing an emission point somewhere:

$$\boldsymbol{u}_j = (\boldsymbol{s}_0^{(j)}, \boldsymbol{s}_1^{(j)}, \ldots, \boldsymbol{s}_{S+1}^{(j)}) \quad \text{where } \boldsymbol{s}_0^{(j)} = \boldsymbol{z}_1 \text{ and } \boldsymbol{s}_{S+1}^{(j)} = \boldsymbol{z}_2.$$

For example, if $S = 1$ i.e. we consider single scattering, then $\boldsymbol{u}_j = (\boldsymbol{z}_1, \boldsymbol{s}^{(j)}, \boldsymbol{z}_2)$.

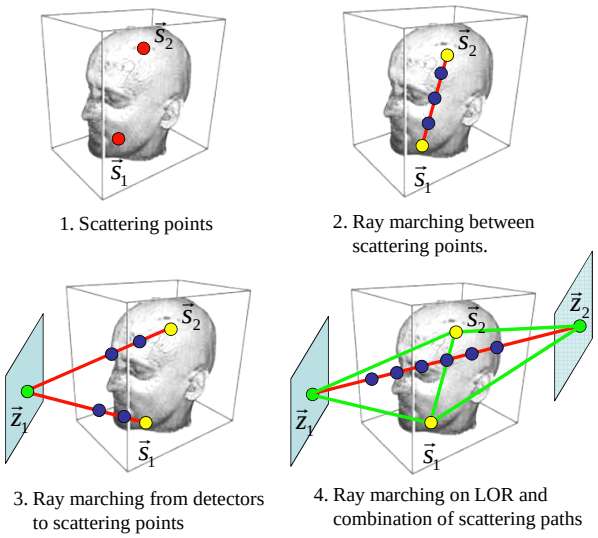

Fig. 2. Steps of the sampling process.

As the computation of a single segment of such a path requires ray-marching and therefore is rather costly, we reuse the segments of a path in many other path samples. The basic steps of the path sampling process are shown by Fig. 2:

1. First, $N_{scatter}$ scattering points $\boldsymbol{s}_1, \ldots, \boldsymbol{s}_{N_{scatter}}$ are sampled.

2. In the second step global paths are generated. If we decide to simulate paths of at most S scattering points, N_{path} ordered subsets of the scattering points are selected and paths of S points are established. If statistically independent random variables were used to sample the scattering points, then the first path may be formed by points $\boldsymbol{s}_1, \ldots, \boldsymbol{s}_S$, the second by $\boldsymbol{s}_{S+1}, \ldots, \boldsymbol{s}_{2S}$, etc. Each path contains $S-1$ line segments, which are marched assuming that the photon energy has not changed from the original electron energy. Note that building a path of length S, we also obtain many shorter paths as well. A path of length S can be considered as two different paths of length $S-1$ where one of the end points is removed. Taking another example, we get $S-1$ number of paths of length 1. Concerning the cost, rays should be marched only once, so the second step altogether marches on $N_{path}(S-1)$ rays.
3. In the third step, each detector is connected to each of the scattering points in a deterministic manner. Each detector is assigned to a computation thread, which marches along the connection rays. The total rays processed by the third step is $N_{det}N_{scatter}$.
4. Finally, detector pairs are given to GPU threads that compute the direct contribution and combine the scattering paths ending up in them. The direct contribution needs altogether $N_{detline}N_{LOR}$ ray-marching computations.

The described sampling process generates point samples. As these point samples are connected to all detectors, paths of length 2 (single scattering, $S = 1$) can be obtained from them. Paths longer than 2, i.e. simulating at least double scattering requires the formation of global paths. The integral quadrature of equation (4) is evaluated with these samples.

To reduce the variance of the random estimator, we should find a sampling density p that mimics the integrand. When inspecting the integrand, we should take into account that we evaluate a set of integrals (i.e. an integral for every LOR) using the same set of global samples, so the density should mimic the common factors of all these integrals. These common factors are the electron density $C(\boldsymbol{v})$ of the scattering points, so we mimic this function when sampling points. We store the scattering cross section at the energy level of the electron, $\sigma(\boldsymbol{v}, 1)$, which is proportional to the electron density. As the electron density function is provided by the CT reconstruction as a voxel grid, we, in fact, sample voxels. The probability density of sampling point $\boldsymbol{v}$ is:

$$p(\boldsymbol{v}) = \frac{\sigma_s(\boldsymbol{v}, 1)}{\int_{\mathcal{V}} \sigma_s(\boldsymbol{v}, 1)\mathrm{d}v} = \frac{\sigma_s[V]}{\mathcal{C}} \frac{N_{voxel}}{\mathcal{V}},$$

where $\sigma_s[V]$ is the scattering cross section at the energy level of the electron in voxel V, $\mathcal{C} = \sum_{V=1}^{N_{voxel}} \sigma_s[V]$ is the sum of all voxels, and $\mathcal{V}$ is the volume of interest.

5 Results

The presented algorithm have been implemented in CUDA and run on nVidia GeForce 480 GFX GPUs. We have modeled the PET system of *NanoPET/CT*

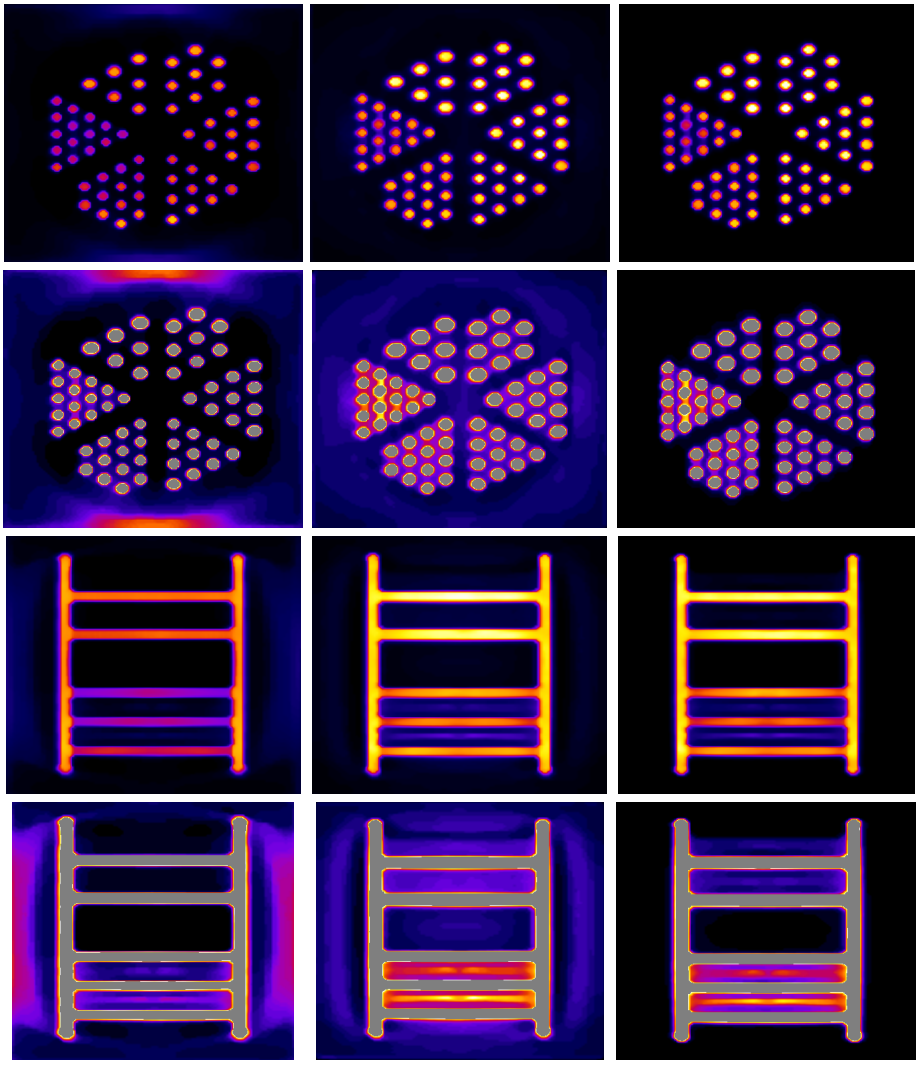

Fig. 3. Reconstruction results of the Derenzo phantom. The upper two rows depict a coronal and a sagittal slice of the reconstructed data, densities shown in the lower two rows are scaled by 5 in order to highlight the differences.

[Med] consisting of twelve square detector modules organized into a ring, and the system measures LORs connecting a detector to three other detectors being at the opposite sides of the ring, which means that $12 \times 3/2 = 18$ module pairs need to be processed. Each of the 12 detector modules consists of 81×39 crystals, thus $N_{det} = 12 \cdot (81 \times 39)$.

The computation effort can be analyzed by counting the number N_{ray} of rays needed to march on, which is

$$N_{ray} = N_{path}(S-1) + N_{det}N_{scatter} + N_{detline}N_{LOR}.$$

In our particular case $S = 1$, $N_{scatter} = 128$, and $N_{detline} = 4$, thus — thanks to the heavy reuse of rays — scatter compensation requires just slightly more rays than the $N_{detline}N_{LOR}$ rays of the unscattered contribution computation.

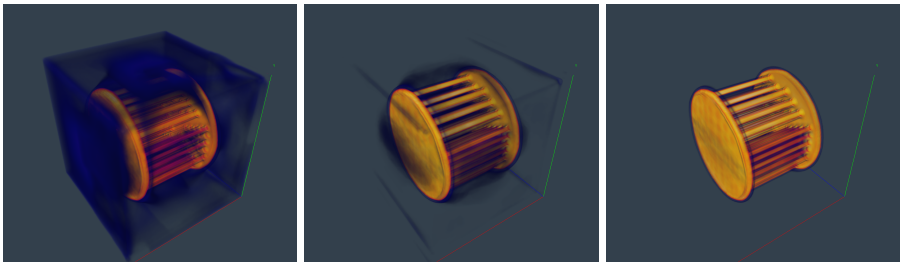

Geometry only | Absorption compensation | Scatter compensation

Fig. 4. 3D views of the Derenzo phantom reconstructions. We used a transfer function that emphasizes the cold noise in blue to make the differences more noticeable.

The reconstruction algorithm is an iteration of photon transfer simulation and density correction. We compared different options during the transfer simulation like computing only the geometry factors, adding the attenuation due to out-scattering and photoelectric absorption, and finally scattering compensation. To compute single scattering, 128 scattering points are used, which are re-sampled in each iteration step. The algorithm has been tested on a Derenzo phantom that contains pipes with radioactive material. The Derenzo phantom is put in a cube of "super bone" of edge length 32 [mm]. Super bone has the same chemical compounds as the normal bone but it is ten times denser. In fact, it is even denser than steal, thus it can emphasize scattering and absorption phenomena. The results of the different options after 100 iteration steps are shown in Fig. 3 and Fig. 4. Note that getting the forward-projection to simulate more of the underlying physical process, the reconstruction can be made more accurate.

6 Conclusion

This paper proposed a GPU based scatter compensation algorithm for the reconstruction of PET measurements. The approach is restructured to exploit the massively parallel nature of GPUs. Based on the recognition that the requirements of the GPU prefer a detector oriented viewpoint, we solve the adjoint problem, i.e. originate photon paths in the detectors. The detector oriented viewpoint also allows us to reuse samples, that is, we compute many annihilation events with tracing a few line segments. The resulting approach can reduce the computation time of the fully 3D PET reconstruction to a few minutes.

Acknowledgement

This work has been supported by the TeraTomo project of the NKTH, OTKA K-719922 (Hungary), and Bulgarian NSF DTK 02/44. This work is connected to the scientific program of the "Development of quality-oriented and harmonized R+D+I strategy and functional model at BME" project. This project is supported by the New Hungary Development Plan (Project ID: TMOP-4.2.1/B-09/1/KMR-2010-0002).

References

[ABB+04] K. Assié, V. Breton, I. Buvat, C. Comtat, S. Jan, M. Krieguer, D. Lazaro, Ch. Morel, M. Rey, G. Santin, L. Simon, S. Staelens, D. Strul, J.-M. Vieira, and R. V. D. Walle. Monte carlo simulation in PET and SPECT instrumentation using GATE. *Nuclear Instruments and Methods in Physics Research Section A*, 527(1–2):180–189, 2004.

[EHV+06] S. Espana, J. L. Herraiz, E. Vicente, J. J. Vaquero, M. Desco, and J. M. Udias. PeneloPET, a Monte Carlo PET simulation toolkit based on PENELOPE: Features and validation. In *IEEE Nuclear Science Symposium Conference*, pages 2597–2601, 2006.

[Gea07] Geant. Physics reference manual, Geant4 9.1. Technical report, CERN, 2007.

[Med] Mediso. http://www.bioscan.com/molecular-imaging/nanopet-ct.

[SK08] L. Szirmay-Kalos. *Monte-Carlo Methods in Global Illumination — Photo-realistic Rendering with Randomization*. VDM, Verlag Dr. Müller, Saarbrücken, 2008.

[SV82] L. Shepp and Y. Vardi. Maximum likelihood reconstruction for emission tomography. *IEEE Trans. Med. Imaging*, 1:113–122, 1982.

[Yan08] C. N. Yang. The Klein-Nishina formula & quantum electrodynamics. *Lect. Notes Phys.*, 746:393–397, 2008.